

Resonance solutions of the nonlinear Schrödinger equation in an open double-well potential

This article has been downloaded from IOPscience. Please scroll down to see the full text article.

2009 J. Phys. B: At. Mol. Opt. Phys. 42 044005

(<http://iopscience.iop.org/0953-4075/42/4/044005>)

View [the table of contents for this issue](#), or go to the [journal homepage](#) for more

Download details:

IP Address: 129.8.242.67

The article was downloaded on 14/05/2010 at 11:24

Please note that [terms and conditions apply](#).

Resonance solutions of the nonlinear Schrödinger equation in an open double-well potential

K Rapedius and H J Korsch

FB Physik, Technische Universität Kaiserslautern, D-67653 Kaiserslautern, Germany

E-mail: korsch@physik.uni-kl.de

Received 10 September 2008, in final form 28 October 2008

Published 3 February 2009

Online at stacks.iop.org/JPhysB/42/044005

Abstract

The resonance states and the decay dynamics of the nonlinear Schrödinger (or Gross–Pitaevskii) equation are studied for a simple, but flexible, model system, the double delta-shell potential. This model allows analytical solutions and provides insight into the influence of the nonlinearity on the decay dynamics. The bifurcation scenario of the resonance states is discussed as well as their dynamical stability properties. A discrete approximation using a biorthogonal basis is suggested which allows an accurate description even for only two-basis states in terms of a nonlinear, non-Hermitian matrix problem.

(Some figures in this article are in colour only in the electronic version)

1. Introduction

In quantum dynamics metastable states can be conveniently described as resonance states, i.e. eigenstates of the Schrödinger equation with complex eigenvalues. Such resonances can be efficiently calculated by complex scaling methods [1] or matrix truncation techniques for periodic lattices [2] and found numerous applications. The recent progress of the physics of Bose–Einstein condensates (BECs) stimulated investigations of the role of resonances for such systems, for instance escape from a potential well or decay by loss of condensate particles as was realized in a recent experiment with ultracold molecules in a one-dimensional lattice [3]. Alternative implementations of open systems with interactions include experiments with optical wave guide arrays [4–6].

Here we will consider a (quasi-) one-dimensional configuration described by the nonlinear Schrödinger equation (NLSE) or Gross–Pitaevskii equation (GPE) for the macroscopic condensate wavefunction

$$\left(-\frac{\hbar^2}{2m} \frac{\partial^2}{\partial x^2} + V(x) + g|\psi(x, t)|^2 \right) \psi(x, t) = i\hbar \frac{\partial \psi(x, t)}{\partial t}, \quad (1)$$

where the nonlinear parameter g describes the self-interaction. First applications of complex energy resonance states

extending the complex scaling method to the nonlinear case investigated the decay of a condensate trapped in the celebrated model potential $V(x) \sim (x^2 - \beta) e^{-\alpha x^2}$ [7–9]. However, the definition of a resonance is somewhat ambiguous in the nonlinear case; alternative descriptions based on amplitude ratios in the inner and outer potential regions have also been proposed and applied to simple model systems allowing an analytical treatment [10]. One of these models is the delta-shell potential discussed in section 2.

Related studies explore resonance phenomena observed in transport problems of BECs, for example the transmission through a potential barrier or across a potential well [11–14] which can be explained in terms of an underlying resonance state [13, 14]. Complex resonances have also been used to describe a BEC in accelerated optical lattices by means of nonlinear Wannier–Stark states [15, 16]. Here the potential in (1) is of the form $V_p(x) + Fx$, where $V_p(x)$ is periodic in space. Such systems can also be described in terms of Wannier functions localized on the potential minima, the ‘sites’. In a single-band approximation this leads to a discrete nonlinear Schrödinger (or Gross–Pitaevskii) equation, well known as the discrete self-trapping equation (DST)¹, which is of interest even in its most simple form of only two sites. Alternatively, this equation can be derived starting from a many-particle

¹ A bibliography on the DST is available: <http://www.ma.hw.ac.uk/chris/dst>.

description of a BEC on a discrete lattice by a Bose–Hubbard Hamiltonian, which leads again to the DST equation in the mean-field limit. In such a description, however, the decay has been neglected. It can be re-introduced by opening the system. This can be done in various ways, purely phenomenologically by introducing complex site energies describing decay [17, 18] or more sophisticatedly by taking explicitly the coupling to an environment into account. Recent studies comparing the full many-particle dynamics with the mean-field approximation consider the two-site system (the open ‘dimer’) phenomenologically [17, 18] or using a master equation for the coupling to the environment [19–21] (see also [22–24] for a study of the related Lipkin–Meshkov–Glick model). It should be noted that even the resulting non-Hermitian nonlinear two-level system shows an intricate crossing scenario as discussed, e.g., in [25]. Two-level systems are often used to model double-well potentials realized in various BEC experiments [26–30].

The present paper is devoted to a detailed analysis of a simple model system, the decay behaviour of a BEC in a double delta-shell potential. This open double-well system is on the one hand simple enough to allow an analytic treatment and closed-form approximations and on the other hand it is flexible enough to investigate characteristic phenomena observed in nonlinear double-well dynamics, as self-trapping and the appearance of new eigenvalues through a saddle node bifurcation [31] and their modification due to the decay.

The paper is organized as follows. In section 2 we first discuss the nonlinear single delta-shell potential and derive simple analytic approximations for the resonance position and decay rate which are compared with exact numerical results. These techniques are in section 3 extended to the double delta-shell potential, where the bifurcation scenario of nonlinear resonance states is analysed as well as the decay dynamics. A discrete-basis set expansion is used in section 3.3 to reduce the system to a finite nonlinear, non-Hermitian matrix problem, which yields reasonable results even for a two-state approximation. A Bogoliubov–de Gennes analysis in section 3.4 provides information about the stability of the resonance states. Additional material concerning computational details is presented in an appendix.

2. Single delta-shell

First we consider the case of an open single well, namely the so-called delta-shell potential

$$V(x) = \begin{cases} +\infty & x \leq 0 \\ (\hbar^2/m)\lambda\delta(x-a) & x > 0 \end{cases} \quad (2)$$

with $\lambda > 0$, $a > 0$ and repulsive interaction $g > 0$. This potential and its generalization to three dimensions have been investigated in detail in the context of the linear Schrödinger equation [32–35]. In the context of the GPE it has been considered in [10] in which resonance positions and widths are extracted from real-valued wavefunctions $\psi(x)$, and a resonance is characterized by a maximum of the probability density $|\psi(x)|^2$ inside the potential region $0 \leq x \leq a$.

Here we consider nonlinear resonance states, i.e. eigenstates of the time-independent NLSE with complex eigenvalues $\mu - i\Gamma/2$

$$\frac{\hbar^2}{2m}\psi'' + (\mu - i\Gamma/2 - V)\psi - g|\psi|^2\psi = 0 \quad (3)$$

and purely outgoing (Siebert) boundary conditions (for details see [14]), which enables us to determine both position μ and decay width $\Gamma/2$ of the resonances and to construct an approximation that allows an analytical treatment. Note that the states $\psi(x, t) = \exp[-i(\mu - i\Gamma/2)t/\hbar]\psi(x)$ do *not* satisfy the time-dependent NLSE since their norm is not constant. Instead they provide an adiabatic approximation to the actual time-dependence (see [9, 36] and section 3.2).

The NLSE (3) with Siebert boundary conditions is solved by the ansatz

$$\psi(x) = \begin{cases} I \operatorname{sn}(\varrho x|p) & 0 \leq x \leq a \\ C e^{ikx} & x > a \end{cases} \quad (4)$$

with a Jacobi elliptic sn-function inside and an outgoing plane wave outside the potential well. The parameters have to satisfy $0 \leq p \leq 1$,

$$\mu - i\Gamma/2 = \frac{\hbar^2}{2m}\varrho^2(1+p) = \frac{\hbar^2 k^2}{2m} + g|C|^2 \quad (5)$$

and

$$|I|^2 = \frac{\hbar^2 \varrho^2 p}{gm}. \quad (6)$$

We fix the norm of the wavefunction to unity inside the potential region $0 \leq x \leq a$:

$$1 = \int_0^a |\psi(x)|^2 dx = \frac{\hbar^2 \varrho}{gm}(\varrho a - E(\varrho a|p)), \quad (7)$$

where $E(u|p)$ is the incomplete elliptic integral of the second kind. Note that the NLSE (3) depends on the product $g|\psi|^2$ so that any renormalization $\psi \rightarrow \psi/\sqrt{\int_0^a |\psi(x)|^2 dx}$ of the wavefunction can be compensated by rescaling the interaction strength according to $g \rightarrow g \int_0^a |\psi(x)|^2 dx$. The matching conditions at $x = a$, $\psi(a+) = \psi(a-) = \psi(a)$, $\psi'(a+) - \psi'(a-) = 2\lambda\psi(a)$, yield

$$I \operatorname{sn}(\varrho a|p) = C e^{ika} \quad (8)$$

$$I \varrho \operatorname{cn}(\varrho a|p) \operatorname{dn}(\varrho a|p) + 2\lambda I \operatorname{sn}(\varrho a|p) = ikC e^{ika}. \quad (9)$$

For a strongly repulsive delta-function at $x = a$ we have $|k| \ll \lambda$ and $\operatorname{sn}(\varrho a|p) \approx 0$ so that the decay of the lowest resonances is weak. Thus, we neglect the imaginary part $-\Gamma/2$ of the eigenvalue in equations (5) and (9). For $\lambda \rightarrow \infty$ the wave number ϱ is given by $\varrho = 2nK(p)/a$ ($K(p)$ is the complete elliptic integral of the first kind) so that for weak decay we can assume

$$\varrho = \frac{2nK(p)}{a} + \delta \quad (10)$$

with $\delta < 0$, $|\delta \cdot a| \ll 1$. Expanding the real part of equation (9) up to second order in δ we obtain

$$\delta = \frac{2\lambda a + 1}{2nK(p)(1+p)a} - \sqrt{\left(\frac{2\lambda a + 1}{2nK(p)(1+p)a}\right)^2 + \frac{2}{(1+p)a^2}}. \quad (11)$$

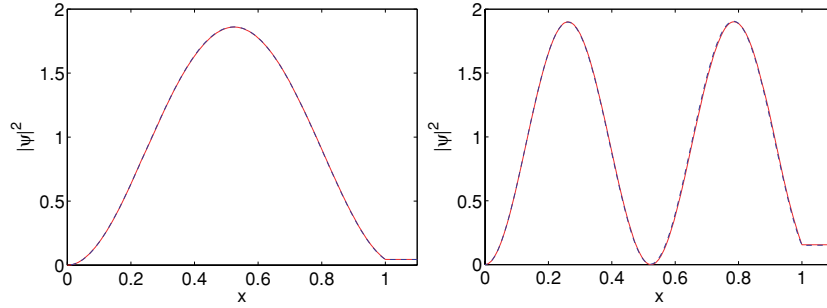


Figure 1. Resonance wavefunction for the ground and first excited states of a delta-shell potential (parameters $\lambda = 10$, $a = 1$ and nonlinearity $g = 1$; units $\hbar = m = 1$). Left: ground state, $n = 1$; right: first excited state, $n = 2$. The exact numerical solutions obtained by the CAP method (dashed blue) are in excellent agreement with the analytical approximations (solid red).

Table 1. Resonance energies $\mu_n - i\Gamma_n/2$ for the two lowest resonances of the delta-shell potential (parameters $\lambda = 10$, $a = 1$ and nonlinearity $g = 1$) calculated analytically (approximation A) and numerically using a grid relaxation method with complex absorbing potentials (CAP).

n	μ_A	μ_{CAP}	$\Gamma_A/2$	$\Gamma_{CAP}/2$
1	5.8950	5.9043	0.0759	0.0751
2	19.4138	19.5065	0.4810	0.4680

For a given value of the Jacobi elliptic parameter $0 \leq p \leq 1$ the real part of the eigenvalue is determined by equations (5), (10) and (11). From the normalization condition (7) the interaction strength is given by

$$g = \frac{\hbar^2 \varrho}{m} (\varrho a - E(\varrho a | p)). \quad (12)$$

The imaginary part of the eigenvalue can be estimated using the Siegert relation [14, 37]:

$$\Gamma/2 = \frac{\hbar^2 k}{2m} \frac{|\psi(a)|^2}{\int_0^a |\psi(x)|^2 dx} = \frac{\hbar^2 k \varrho p}{2m} \frac{\text{sn}^2(\varrho a | p)}{\varrho a - E(\varrho a | p)}. \quad (13)$$

Exact results can be obtained from a numerical calculation combining a complex absorbing potential (CAP) with a grid relaxation. In these computations we use the approximate resonances derived above as starting values. Complex absorbing potentials were shown to be equivalent to exterior complex scaling [1] and successfully applied to resonances of the GPE [7]. A detailed discussion of our particular implementation as well as its application to nonlinear Wannier–Stark resonances will be presented elsewhere [38].

As an example, figure 1 shows the wavefunctions for the ground state and the first excited state of the delta-shell potential (2) with $\lambda = 10$, $a = 1$ and a nonlinearity of $g = 1$ (units with $\hbar = 1 = m$ are used throughout this paper) and table 1 lists the resonance energies. In addition, the analytical approximations derived above are given. Good agreement is observed.

3. Double delta-shell

An open double well allows us to study the influence of the decay on characteristic nonlinear phenomena, such as self-

trapping. Here we investigate a simple case, namely the double delta-shell potential

$$V(x) = \begin{cases} +\infty & x \leq 0 \\ (\hbar^2/m) [\lambda_b \delta(x-b) + \lambda_a \delta(x-a)] & x > 0, \end{cases} \quad (14)$$

which consists of an infinitely high wall and two repulsive delta barriers with strength $\lambda_a > 0$, $\lambda_b > 0$ located at $a > b > 0$. This potential possesses two simpler limits: for $\lambda_a \rightarrow 0$ or $\lambda_b \rightarrow 0$ we recover the single delta-shell potential discussed in section 2. In the limit $\lambda_a \rightarrow \infty$ the system is closed yielding a coherent nonlinear tunnelling oscillation between two (asymmetric) potential wells [31, 39]. For finite values of λ_a we therefore observe non-Hermitian generalizations of these simple cases. The considerations in the following subsection essentially follow those from the preceding section for the single delta-shell potential. We first consider stationary resonance states followed by a discussion of the dynamics and a stability analysis. As in the preceding section we concentrate on repulsive nonlinearities $g > 0$.

3.1. Stationary states

The NLSE (3) with the potential (14) and Siegert boundary conditions is solved by the ansatz

$$\psi(x) = \begin{cases} I_1 \text{sn}(\varrho_1 x | p_1) & 0 \leq x \leq b \\ I_2 \text{sn}(\varrho_2 x + \vartheta | p_2) & b < x \leq a \\ C e^{ikx} & x > a \end{cases} \quad (15)$$

with

$$\begin{aligned} \mu - i\Gamma/2 &= \frac{\hbar^2}{2m} \varrho_1^2 (1 + p_1) = \frac{\hbar^2}{2m} \varrho_2^2 (1 + p_2) \\ &= \frac{\hbar^2 k^2}{2m} + g|C|^2, \end{aligned} \quad (16)$$

$$|I_1|^2 = \frac{\hbar^2 \varrho_1^2 p_1}{gm}, \quad |I_2|^2 = \frac{\hbar^2 \varrho_2^2 p_2}{gm} \quad (17)$$

and $0 \leq p \leq 1$. At $x = a$ we obtain the matching conditions

$$I_2 \text{sn}(\varrho_2 a + \vartheta | p_2) = C e^{ika} \quad (18)$$

$$\begin{aligned} I_2 \varrho_2 \text{cn}(\varrho_2 a + \vartheta | p_2) \text{dn}(\varrho_2 a + \vartheta | p_2) \\ + 2\lambda_a I_2 \text{sn}(\varrho_2 a + \vartheta | p_2) = ikC e^{ika}. \end{aligned} \quad (19)$$

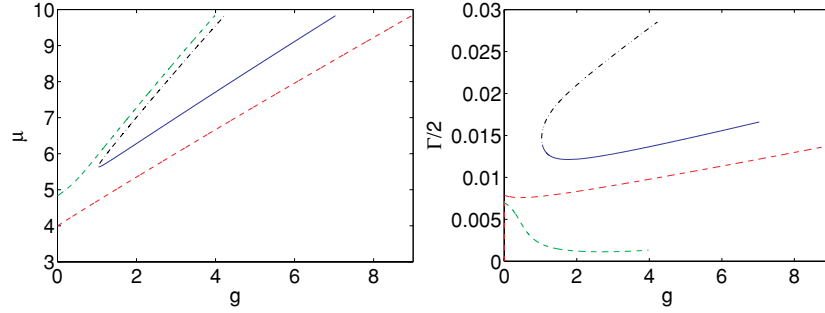


Figure 2. Analytically calculated bifurcation diagrams for the parameters $\lambda_b = 10$, $\lambda_a = 20$, $b = 1$ and $a = 2$. Left panel: chemical potentials. Right panel: decay rates.

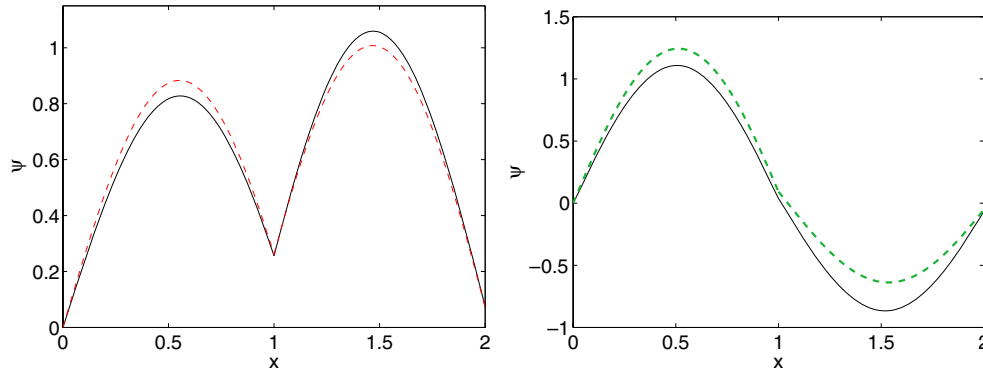


Figure 3. Wavefunctions of the two lowest states for $\lambda_b = 10$, $\lambda_a = 20$, $b = 1$, $a = 2$. Left panel: ground state for $g = 0$ (solid black) and $g = 0.5$ (dashed red). Right panel: first excited state for $g = 0$ (solid black) and $g = 0.5$ (dashed green).

Due to the repulsive delta-function at $x = a$ we have $k \ll \lambda_a$ and $\text{sn}(q_2 a + \vartheta | p_2) \approx 0$. As in the previous section we neglect the decay coefficient $\Gamma/2$ in equation (19). Furthermore, we assume $q_2 a + \vartheta = 4nK(p_2) + \delta \cdot a$ with $\delta \cdot a < 0$, $|\delta \cdot a| \ll 1$. Expanding the real part of equation (19) up to second order in δ we obtain

$$\delta = \frac{2\lambda_a a}{q_2(1+p_2)a^2} - \sqrt{\left(\frac{2\lambda_a a}{q_2(1+p_2)a^2}\right)^2 + \frac{2}{(1+p_2)a^2}} \quad (20)$$

so that the phase shift is given by $\vartheta = 4nK(p_2) + \delta \cdot a - q_2 a$.

The matching conditions at $x = b$ read

$$I_1 \text{sn}(u_1 | p_1) = I_2 \text{sn}(u_2 | p_2), \quad (21)$$

$$I_1 q_1 \text{cn}(u_1 | p_1) \text{dn}(u_1 | p_1) + 2\lambda_b I_1 \text{sn}(u_1 | p_1) = I_2 q_2 \text{cn}(u_2 | p_2) \text{dn}(u_2 | p_2) \quad (22)$$

where $u_1 = q_1 b$, $u_2 = q_2 b + \vartheta$. By inserting equation (21) into (22) and using the relations between the squares of the Jacobi elliptic functions we arrive at

$$\begin{aligned} \frac{p_1}{(p_1+1)^2} &= \frac{p_2}{(p_2+1)^2} - \frac{p_2}{(p_2+1)^{3/2}} \frac{4\lambda_b}{\sqrt{2\mu}} \\ &\times \text{sn}(u_2 | p_2) \text{cn}(u_2 | p_2) \text{dn}(u_2 | p_2) \\ &+ \frac{2\lambda_b^2}{\mu} \frac{p_2}{p_2+1} \text{sn}(u_2 | p_2)^2 = F(p_2, \mu) \end{aligned} \quad (23)$$

so that the parameter p_1 is given by

$$p_1 = \frac{1}{2F} - 1 - \sqrt{\left(\frac{1}{2F} - 1\right)^2 - 1}. \quad (24)$$

From equations (20)–(24) all relevant quantities are known in terms of p_2 and μ . To calculate the eigenvalues we solve equation (22) for a given value of μ and thus obtain up to four solutions for p_2 in $[0, 1]$.

From the normalization condition $\int_0^a |\psi(x)|^2 dx = 1$ we can determine the interaction parameter

$$g = \frac{\hbar^2}{m} [q_1(q_1 b - E(q_1 b | p_1)) + q_2(q_2(a-b) + E(q_2 b + \vartheta | p_2) - E(q_2 a + \vartheta | p_2))]. \quad (25)$$

The decay coefficient is again estimated by the Siegert relation

$$\Gamma/2 = \frac{\hbar^2 k}{2m} \frac{|\psi(a)|^2}{\int_0^a |\psi(x)|^2 dx}. \quad (26)$$

As an example we consider the lowest eigenstates of the potential with parameters $\lambda_b = 10$, $\lambda_a = 20$, $b = 1$ and $a = 2$. Figure 2 shows the real and imaginary parts of the eigenvalues in dependence of the nonlinear parameter g . The two lowest eigenvalues μ of the linear ($g = 0$) system (dashed green and dashed red) increase almost linearly with increasing repulsive interaction strength g . The corresponding wavefunctions are shown in figures 3 and 4 for $g = 0, 0.5$ and 3. For a weak nonlinearity (figure 3) the ground state is almost symmetric and the first excited state is almost antisymmetric. These states with linear counterpart are referred to as *autochthonous* states. At $g \approx 1$ two new eigenvalues appear through a saddle node bifurcation (cf [31]) which we will henceforth call *allochthonous* states. One of these

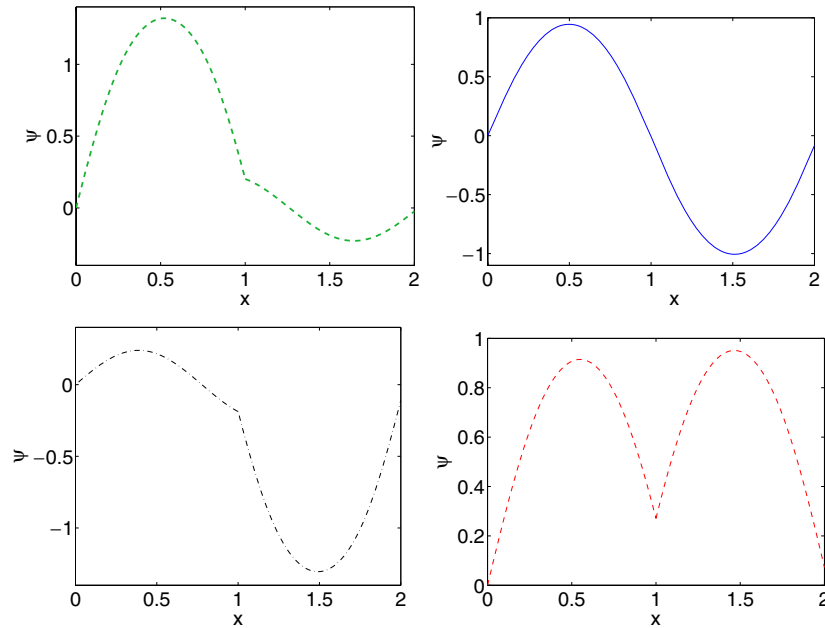


Figure 4. Analytically calculated wavefunctions for $\lambda_b = 10$, $\lambda_a = 20$, $b = 1$, $a = 2$ and $g = 3$. Upper left: autochthonous self-trapping state (AuT); lower left: allochthonous self-trapping state (AIT); upper right: allochthonous almost antisymmetric state (Al-); lower right: autochthonous almost symmetric state (Au+).

two states is dynamically stable (dashed-dotted black) and the other is unstable (solid blue) (see subsection 3.2). After the bifurcation the state which was almost antisymmetric before the bifurcation (dashed green) localizes more and more in the left well with increasing interaction, whereas the newly created state (dashed-dotted black) localizes in the right well (see upper left and lower left panels of figure 4). These two symmetry breaking states are referred to as autochthonous self-trapping states (AuT) and allochthonous self-trapping states (AIT), respectively. The two remaining states are referred to as the autochthonous almost symmetric state (Au+) (dashed red) and allochthonous almost antisymmetric state (Al-) (solid blue) (see upper right and lower right panels of figure 4).

The imaginary parts of the eigenvalues, the decay widths $\Gamma/2$, shown in the right panel of figure 2 grow with increasing interaction strength g for large values of g . This behaviour can be understood via the Siegert formula (26) which predicts a dependence $\Gamma/2 \propto \sqrt{\mu}$, if the shape of the wavefunction does not change much with μ (respectively g) and furthermore μ is proportional to g in this parameter range (cf left panel of figure 2). For small values of g , the decay coefficient of the autochthonous self-trapping state (dashed green) decreases rapidly with increasing g because of the increasing localization of the wavefunction in the left well, where the probability for tunnelling out of the barrier region $0 \leq x \leq a$ is small.

For comparison we consider the limit $\lambda_a \rightarrow \infty$ in which the system becomes both symmetric and Hermitian. Similar systems have recently been considered in a number of papers [31, 39–41]. Naturally the analytical results obtained in this limit are exact. From equation (20) we see that in this case we have $\delta = 0$ and all eigenvalues are real. In the upper left panel of figure 5 the chemical potential μ is plotted

in dependence of the interaction strength g . Compared to the non-Hermitian nonsymmetric case considered before the saddle node bifurcation has changed to a pitchfork bifurcation, since the eigenvalues of the two self-trapping states now coincide due to the symmetry of the system (cf [31]). One of these states is shown in the lower left panel of figure 5, the other one is obtained by mirroring at the axis $x = b$. Hence the respective eigenvalues, indicated by the dashed-dotted black curve, are degenerate after the bifurcation. The two remaining eigenstates (lower right and upper right panels) are now genuinely symmetric, respectively antisymmetric.

As in the case of the open single well, we compare our approximate analytical results for the resonance solutions of the open double well with numerically exact ones calculated using a grid relaxation method with complex absorbing potentials (see section 2). The results are given in figure 6 and table 2. For the two autochthonous states, we observe good agreement between the analytical approximation and the numerically exact solutions. For the AIT state (dashed-dotted black), the grid relaxation only converges for high values of g (respectively μ) but wherever it converges there is good agreement between the analytical approximation and the numerically exact solutions. For the Al- state (solid blue) the grid relaxation does not converge at all. It turns out (see sections 3.2 and 3.4) that this state is dynamically unstable just like the respective state in the asymmetric Hermitian double well (see [31]).

At the bifurcation point the real and imaginary parts of the eigenvalues of the allochthonous states both coincide. By computing the overlap of the two respective wavefunctions (figure 7) one can demonstrate that the wavefunctions also coincide at the bifurcation point. Thus, the bifurcation point is an example of an *exceptional* point (see [17, 42, 43]).

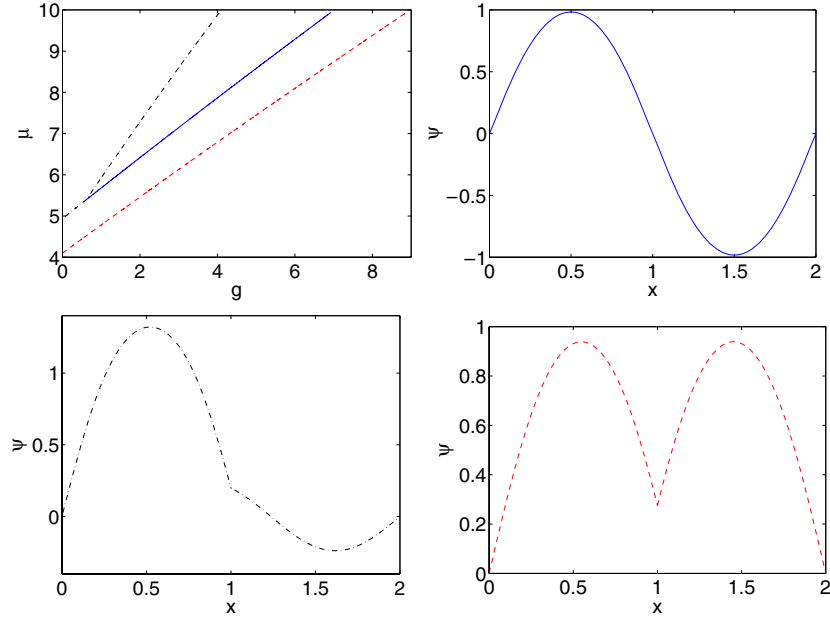


Figure 5. Analytical results for $\lambda_b = 10, \lambda_a \rightarrow \infty, b = 1, a = 2$. Upper left panel: bifurcation diagram. The other panels show eigenstates for $g = 3$. Lower left: self-trapping state; upper right: antisymmetric state; lower right: symmetric state.

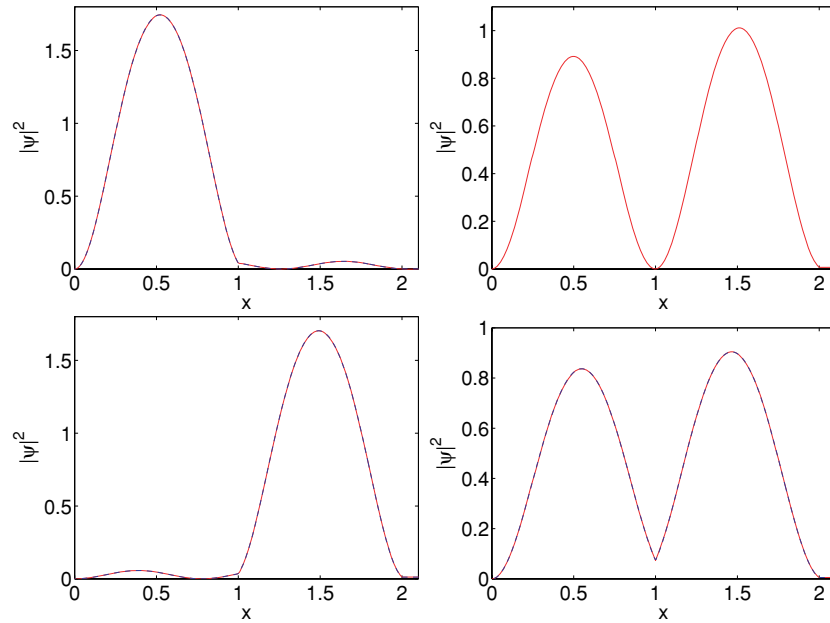


Figure 6. Comparison between the squared magnitudes of the analytically calculated eigenstates (solid red) and the numerically exact solution obtained by the CAP method (dashed blue) for the same states as in figure 4; i.e. upper left: autochthonous self-trapping state (AuT); lower left: allochthonous self-trapping state (AIT); upper right: allochthonous almost antisymmetric state (AI-); lower right: autochthonous almost symmetric state (Au+). On the scale of drawing, the results of the two methods are almost indistinguishable.

Table 2. Chemical potential and decay rates for the same states as in figure 6. The approximate analytical values (A) are compared with numerically exact ones (CAP) calculated by a grid relaxation method with complex absorbing potentials.

Eigenstate	μ_A	$\Gamma_A/2$	μ_{CAP}	$\Gamma_{CAP}/2$
Autochthonous self-trapping state (AuT)	8.589	0.00114	8.588	0.00114
Allochthonous self-trapping state (AIT)	8.301	0.02453	8.303	0.02443
Allochthonous almost antisymmetric state (AI-)	6.999	0.01279		
Autochthonous almost symmetric state (Au+)	6.014	0.00902	6.014	0.00900

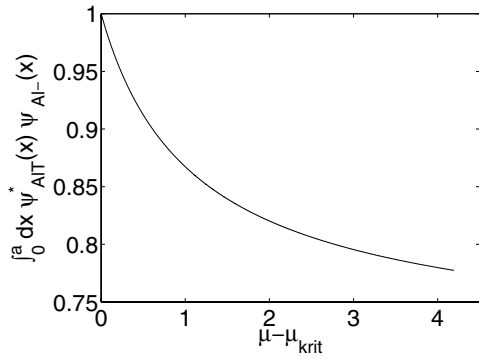


Figure 7. Overlap of the two allochtonous states for the parameters $\lambda_b = 10$, $\lambda_a = 20$, $b = 1$ and $a = 2$.

3.2. Dynamics

The eigenstates calculated in the preceding subsection have complex eigenvalues and are hence subject to decay. Following [9, 36] we call an eigenstate *dynamically stable* if its time evolution follows the stationary adiabatic decay behaviour given by

$$\partial_t (g_{\text{eff}}) = -\Gamma(g_{\text{eff}})g_{\text{eff}}, \quad (27)$$

where $g_{\text{eff}} = gN$ with $N = \int_0^a |\psi(x)|^2 dx$ denotes the effective nonlinear interaction inside the double-well potential [10]. In subsection 3.1 the total norm was kept fixed at $N = 1$ and g was varied. Now we keep g fixed whereas N decreases due to decay. We compute the time evolution of the states shown in figure 4 using a Crank–Nicholson propagation with a predictor–corrector algorithm and absorbing boundaries [13, 44].

The results are given in figures 8–11 each of which shows a spatio-temporal contour plot of the density $|\psi(x, t)|^2$ (left panel), the relative population of the two wells (upper right panel) and the decay of the norm N (lower right panel) which is calculated directly via time evolution (dashed blue curve) and compared to the stationary decay behaviour according to equation (27) (solid red curve) calculated from the stationary eigenvalues shown in figure 2. The time evolution of the

autochtonous states (figures 8 and 11) closely follows the stationary decay behaviour. Thus these states are dynamically stable. The relative population of the state Au+ (upper right panel of figure 11) reveals a small oscillation in addition to the adiabatic evolution, which can be explained by a linear stability analysis based on the Bogoliubov–de Gennes equations (see section 3.4).

If the time evolution is initiated with the almost antisymmetric allochtonous state (Al–, figure 9), the wavefunction starts to oscillate between the wells and hence does not exhibit the stationary decay behaviour so that it is termed dynamically unstable. Due to the asymmetry of the system there is no complete population transfer between the wells. Because of the influence of interaction the Josephson oscillations for small times are not sine-shaped but can be described by a Jacobi elliptic function (see, e.g., [39] and references therein). For longer times, the effective nonlinearity decreases due to the decay so that the oscillation becomes more sine-shaped and its period slowly gets closer to the value $2\pi\hbar/\Delta\mu_{g=0} \approx 7.53$ for the Josephson oscillations of the linear system, where $\Delta\mu_{g=0} \approx 0.834$ is the difference between the chemical potentials of the ground and first excited states for $g = 0$ (cf figure 3). In order to estimate the oscillation period for short times we consider the interval between the first two population maxima in the left well at $t_1 \approx 4.05$ and $t_2 \approx 10.84$. In an *ad hoc* approach we take the interaction into account by considering the difference between the chemical potentials of the almost symmetric, respectively antisymmetric quasistationary eigenstates Au+ and Al– in the middle of the interval $[t_1, t_2]$ instead of $\Delta\mu_{g=0}$. In the middle of the interval $[t_1, t_2]$, we still have about 80% of the initial population left so that the effective nonlinearity can be estimated as $g_{\text{eff}} \approx 2.4$ and the respective difference between the chemical potentials is approximately given by $\Delta\mu_{g=2.4} \approx 0.95$ (cf figure 2). The resulting estimate for the period $2\pi\hbar/\Delta\mu_{g=2.4} \approx 6.6$ roughly agrees with the value $t_2 - t_1 \approx 6.79$ observed in the dynamical calculation.

The time evolution of the allochtonous self-trapping state (AIT, figure 10) follows the stationary decay behaviour until the bifurcation point is reached. After that it tunnels

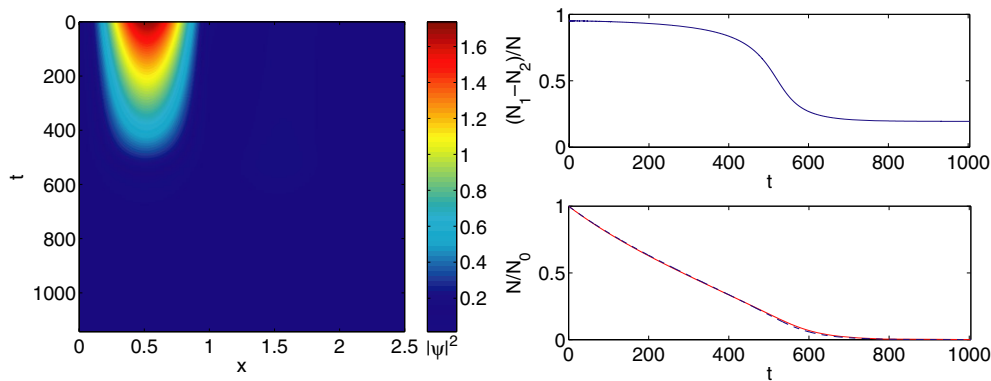


Figure 8. Time evolution of the autochtonous self-trapping state (AuT) from figure 4. Left panel: spatio-temporal contour plot of the density $|\psi(x, t)|^2$. Upper right panel: relative population of the two wells. N_1 and N_2 denote the total norm inside the left and right wells, respectively. Lower right panel: decay of the norm N of the wavefunction inside the double barrier calculated via time evolution (dashed blue) and using stationary states (solid red). N_0 is the norm at $t = 0$.

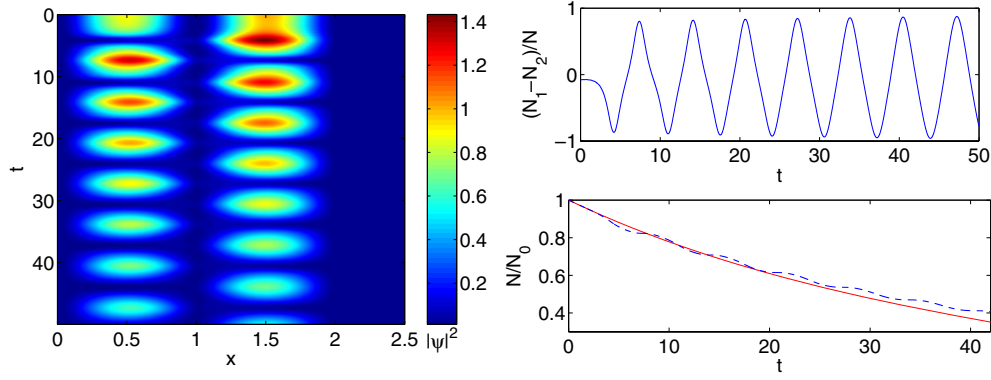


Figure 9. The same as figure 8, however, for the allochthonous almost antisymmetric state (Al-).

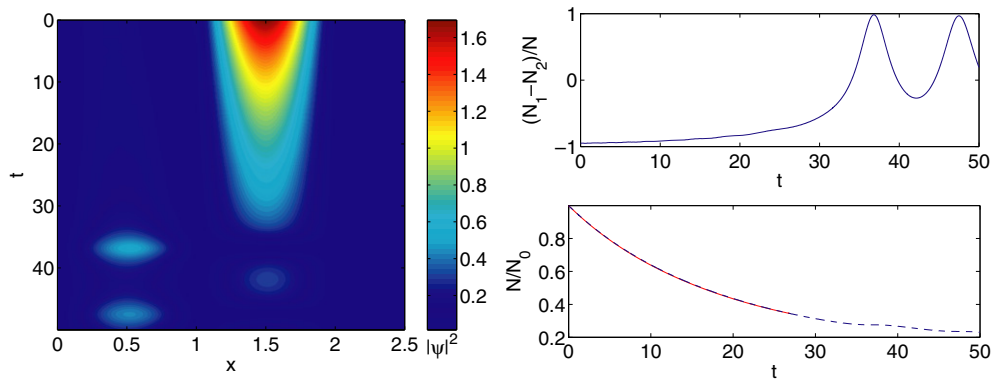


Figure 10. The same as figure 8, however, for the allochthonous self-trapping state (AIT).

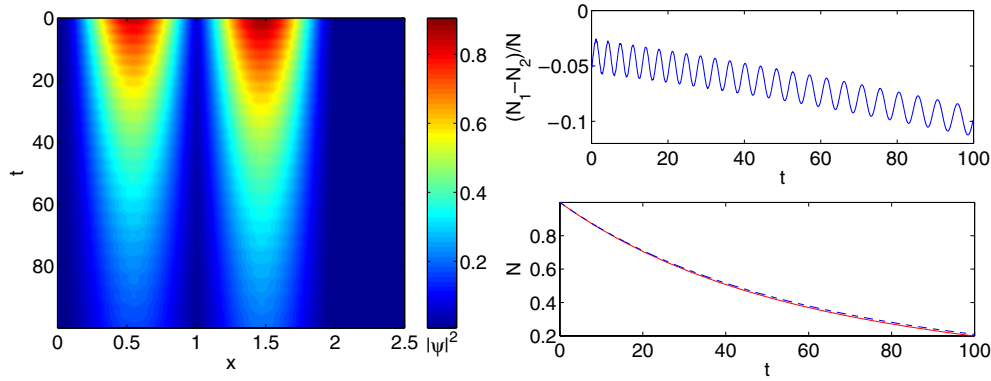


Figure 11. The same as figure 8, but for the autochthonous almost symmetric state (Au+).

completely from the right to the left well and starts oscillating between total population of the left well and an intermediate population of the two wells. This asymmetry indicates that a part of the total population of the double well does not take part in the oscillation but is trapped in the AuT state.

In conclusion, we observe that there are dynamically stable states whose dynamics is well described by stationary states in an adiabatic approximation. In particular, the self-trapping effect is not immediately destroyed by decay but survives until the bifurcation point is reached. Especially in the autochthonous self-trapping state (AuT) the trapping can be preserved for a long time since this state decays very slowly.

3.3. Finite-basis approximation

Instead of solving the NLSE as a differential equation, one can, in a Galerkin-type ansatz, expand the wavefunction $\psi(x, t) = \exp(-i(\mu - i\Gamma/2)t/\hbar)u(x, t)$ as

$$u(x, t) = \sum_{j=1}^{n_B} c_j(t)u_j(x) \quad (28)$$

using the first n_B eigenfunctions $\{u_j\}$ and respective eigenvalues $\{\mu_j - i\Gamma_j/2\}$ of the corresponding linear ($g = 0$) system with the Hamiltonian

$$H_0 = -\frac{\hbar^2}{2m}\partial_x^2 + V(x) \quad (29)$$

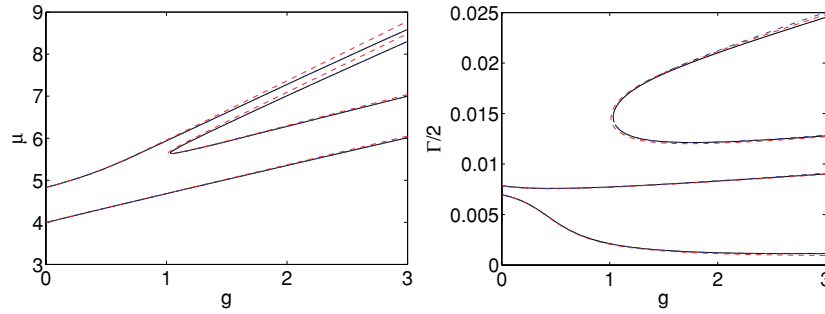


Figure 12. Bifurcation diagram for $\lambda_b = 10$, $\lambda_a = 20$, $b = 1$, $a = 2$. Solid black: analytical result (cf figure 2); dashed red: Galerkin approximation with $n_B = 2$ modes; dashed-dotted blue: $n_B = 30$ modes.

using Siegert boundary conditions. The NLSE can now be written as

$$i\hbar\partial_t u = (H_0 - (\mu - i\Gamma/2))u + g|u|^2 u. \quad (30)$$

Since H_0 is not Hermitian the states $\{u_j\}$ are not orthogonal. Instead they form a *finite*-basis set

$$\int_0^\infty v_j^*(x)u_l(x) dx = \delta_{jl} \quad (31)$$

together with the eigenvectors $\{v_j\}$ of the adjoint Hamiltonian H_0^\dagger satisfying

$$H_0^\dagger v_j = (\mu_j - i\Gamma_j/2)^* v_j, \quad (32)$$

the so-called *left eigenvectors* of H_0 (see, e.g., [45]). We compute the left and right eigenvectors using exterior complex scaling in order to make the states $\{u_j\}$ and $\{v_j\}$ square integrable in $0 \leq x \leq \infty$ (see the appendix).

To calculate the stationary states we set $\partial_t u_j = 0$, $1 \leq j \leq n_B$, and consider the projections of equation (30) on the n_B left eigenvectors:

$$c_j(E_j - E) + g \int_0^\infty dx v_j^*(x) \left| \sum_{i=1}^{n_B} c_i u_i(x) \right|^2 \sum_{l=1}^{n_B} c_l u_l(x) = 0, \quad 1 \leq j \leq n_B \quad (33)$$

with $E = \mu - i\Gamma/2$ and $E_j = \mu_j - i\Gamma_j/2$. Together with the normalization condition

$$\int_0^a dx |u(x)|^2 = 1 \quad (34)$$

and a condition

$$\arg(u(a)) = 0 \quad (35)$$

which fixes the phase of the wavefunction we obtain a system of nonlinear equations for the coefficients $\{c_j\}$, the chemical potential μ and the decay rate Γ . This system (33)–(35) is solved with a Newton algorithm.

Alternatively, equation (33) can be rewritten as

$$c_j(E_j - E) + \sum_{ik\ell=1}^{n_B} w_{k\ell}^{ji} c_i^* c_k c_\ell = 0 \quad (36)$$

with

$$w_{k\ell}^{ji} = g \int_0^\infty dx v_j^*(x) u_i^*(x) u_k(x) u_\ell(x) = w_{\ell k}^{ji}, \quad (37)$$

where the integrations can be carried out once in the beginning. This has some advantages for small n_B . For the most simple case of only two states this yields the nonlinear, non-Hermitian 2×2 eigenvalue equation

$$\begin{pmatrix} E_1 - E + \kappa_{11} & \kappa_{12} \\ \kappa_{21} & E_2 - E + \kappa_{22} \end{pmatrix} \begin{pmatrix} c_1 \\ c_2 \end{pmatrix} = 0 \quad (38)$$

with

$$\kappa_{11} = w_{11}^{11} |c_1|^2 + 2w_{12}^{12} |c_2|^2 + w_{11}^{12} c_2^* c_1 \quad (39)$$

$$\kappa_{12} = w_{11}^{22} |c_2|^2 + 2w_{11}^{12} |c_1|^2 + w_{11}^{21} c_1^* c_2 \quad (40)$$

$$\kappa_{21} = w_{21}^{11} |c_1|^2 + 2w_{21}^{21} |c_2|^2 + w_{21}^{12} c_2^* c_1 \quad (41)$$

$$\kappa_{22} = w_{22}^{22} |c_2|^2 + 2w_{22}^{21} |c_1|^2 + w_{22}^{21} c_1^* c_2. \quad (42)$$

In figure 12 we compare the bifurcation diagram calculated in section 3.1 (solid black lines) with the Galerkin approach with $n_B = 2$, (dashed red lines) and $n_B = 30$ modes (dashed-dotted blue lines). Both real (left panel) and imaginary (right panel) parts of the eigenvalues are reasonably well reproduced by such a two mode approximation. Naturally the agreement is best for the two lowest states. The Galerkin approximation with $n_B = 30$ modes almost coincides with the results from section 3.1 in the displayed parameter range $0 \leq g \leq 3$, except for the decay coefficient of the allochthonous self-trapping state for high values of g . In order to achieve such a good agreement, it is essential to use the biorthogonal basis. If only the right eigenvectors are used, i.e. if we project equation (30) on the $\{u_j\}$ instead of the $\{v_j\}$, the results are worse. Figure 13 reveals that for $n_B = 2$ modes the real parts of the eigenvalues are still in good agreement with the analytical results whereas the imaginary parts of the eigenvalues clearly differ from the previous results, since the growth of the decay rates with increasing nonlinearity g (cf the discussion in section 3.1) is not reproduced. The results for $n_B = 10$ demonstrate that the agreement improves if higher modes are taken into account. Thus the decay rates are much more sensitive to the excitation of higher modes than the real parts of the eigenvalues. The agreement can be improved if we calculate the decay rates with the Siegert formula (26) using the wavefunctions and real parts of the respective eigenvalues calculated with the $n_B = 2$ (red dots) and the $n_B = 10$ (blue dots) Galerkin approximation.

These results indicate that the biorthogonal basis $\{v_j\}, \{u_j\}$ is better suited to describe the system than $\{u_j\}$ alone. Naturally the differences between different choices of basis sets disappear in the limit $n_B \rightarrow \infty$.

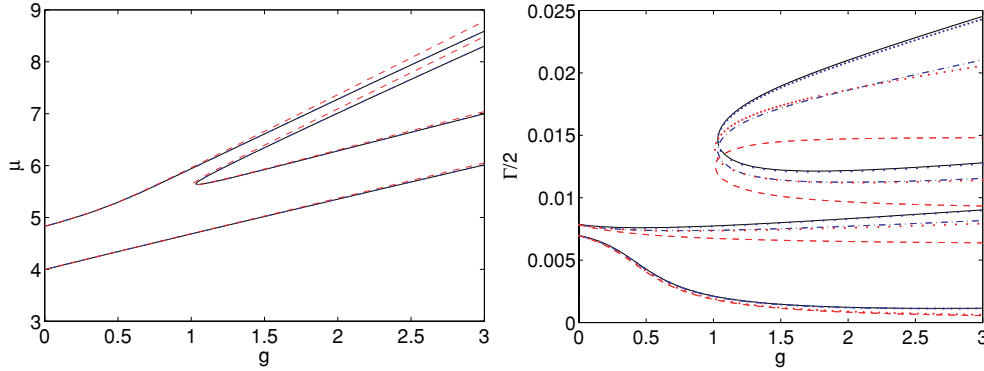


Figure 13. Bifurcation diagram for $\lambda_b = 10$, $\lambda_a = 20$, $b = 1$, $a = 2$ and projection onto the right eigenvectors $\{u_j\}$. Solid black: analytical result (cf figure 2); dashed red: Galerkin approximation with $n_B = 2$ modes; red dots: $n_B = 2$ modes and Siegert formula; dashed-dotted blue: $n_B = 10$ modes; blue dots: $n_B = 10$ modes and Siegert formula.

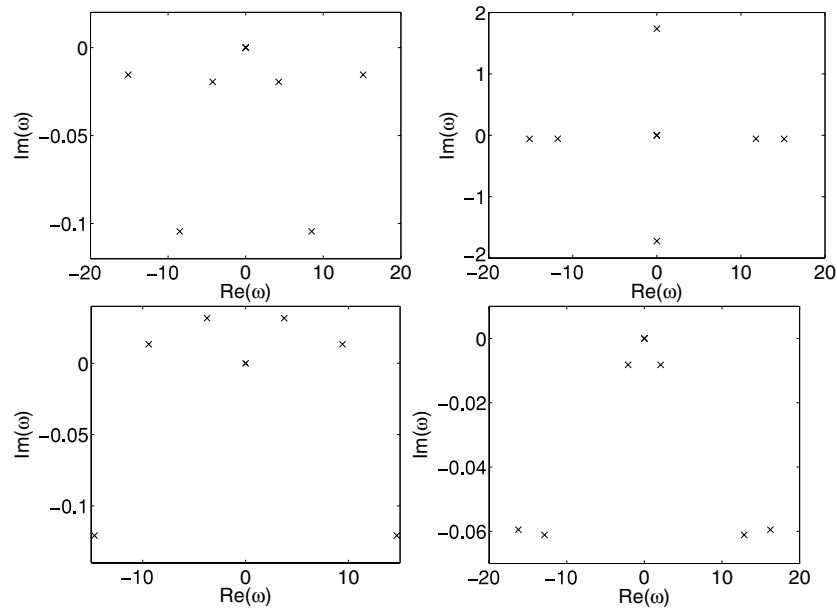


Figure 14. Bogoliubov excitation spectra for the same parameters as in figure 4 computed with $n_B = 4$ basis functions. Upper left: autochthonous self-trapping state (AuT); lower left: allochthonous self-trapping state (AIT); upper right: allochthonous almost antisymmetric state (AI-); lower right: autochthonous almost symmetric state (Au+).

3.4. Linear stability analysis

In this subsection we analyse the stability of the adiabatic time evolution of the quasistationary states by solving the Bogoliubov–de Gennes (BdG) equations and compare its predictions with the results of the dynamical calculations from section 3.2. The BdG equations are obtained by linearizing the GPE in the vicinity of a background solution ψ_0 , i.e. by inserting $\psi = \psi_0 + \delta\psi$ into the GPE and expanding the resulting equation up to first order in $\delta\psi$. Since we are considering quasistationary rather than stationary background solutions we follow the prescription of Castin and Dum [46] for time-dependent background solutions. They argue that only the components $\delta\psi_\perp$ perpendicular to the time-dependent background solution are relevant. Assuming a time dependence $\delta\psi_\perp(t) = \exp[-i(\mu - i\Gamma/2)t/\hbar](\chi_- \exp(-i\omega t) +$

$\chi_+^* \exp(i\omega^* t))$ the BdG equations read in our case

$$\begin{aligned} & \hbar\omega \begin{pmatrix} \chi_- \\ \chi_+ \end{pmatrix} \\ &= \begin{pmatrix} H_{\text{GP}} + gQ|\psi_0|^2Q - E & gQ\psi_0^2Q^* \\ -gQ^*\psi_0^{*2}Q & -H_{\text{GP}}^* - gQ^*|\psi_0|^2Q^* + E^* \end{pmatrix} \\ & \times \begin{pmatrix} \chi_- \\ \chi_+ \end{pmatrix} \end{aligned} \quad (43)$$

with $E = \mu - i\Gamma/2$, where $Q = 1 - |\psi_0\rangle\langle\psi_0|$ is the projector orthogonal to the background state ψ_0 and the Gross–Pitaevskii Hamiltonian $H_{\text{GP}} = H_0 + g|\psi_0|^2$. The population of eigenmodes with positive imaginary part of the eigenvalue grows exponentially in time, thus leading to instability. The eigenvalue equation (43) is solved by expansion in the eigenbasis of H_0 as described in section 3.3. Figure 14 shows the Bogoliubov excitation spectra for the same states as in

figure 4 computed with $n_B = 4$ basis functions. Note that in the figure only seven instead of eight eigenvalues are observed since the eigenvalue zero is doubly degenerated. The results do not change significantly if more basis states are taken into account. The excitation spectrum of the state Al− (upper right panel) has an excitation with zero real part and a large positive imaginary part which leads to instability as observed in the dynamical calculations (cf figure 9). The autochtonous states (upper left and lower right panels) only have excitations with negative imaginary part so that the adiabatic stability seen in the dynamical calculations (figures 8 and 11) is confirmed. The first (nonzero) excitation of the Au+ state (lower right panel) has the eigenvalue $\omega \approx \pm 2.1 - i0.0075$. The small imaginary part indicates that the excitation is only weakly damped. The period $2\pi/|\text{Re}(\omega)| \approx 3$ of the excitation agrees with the period of the small oscillation in the background state's population imbalance (upper right panel of figure 11) for short times. In the limit $g \rightarrow 0$, the nonzero eigenvalues of the BdG equations (43) are given by the differences of the eigenenergies of H_0 so that for longer times the oscillation period slowly approaches the value $2\pi\hbar/\Delta\mu_{g=0} \approx 7.53$ for the Josephson oscillations of the linear system.

The situation is more involved for the excitation spectrum of the allochtonous self-trapping state (AIT) (lower left panel). In the dynamical calculation it seems to evolve adiabatically until the bifurcation point is reached (figure 10). Yet, its excitation spectrum shows eigenvalues with positive imaginary parts. These imaginary parts $\text{Im}(\omega) \approx 0.0317$ are, however, quite small and the characteristic time scale for the growth of the respective excitations can be roughly estimated as $1/\text{Im}(\omega) \approx 32$, which is on the same order of magnitude as the time $\Delta t \approx 30$ that it takes for the dynamical evolution to reach the bifurcation point (cf figure 10). Consequently, the evolution of the eigenstate is approximately adiabatic up to the bifurcation point if the initial population of the destabilizing excitations is small.

4. Conclusion

In this paper we analysed the resonance states and the decay dynamics of the nonlinear Schrödinger equation for a double delta-shell potential.

By means of an approximation the resonance wavefunctions and eigenvalues were calculated analytically. In analogy to the respective closed system the real parts of the eigenvalues in dependence on the nonlinearity g show a saddle node bifurcation as symmetry breaking solutions emerge for a critical value of g . The imaginary parts (decay rates) undergo a similar bifurcation scenario. The approximate analytical results are in good agreement with numerically exact calculations based on complex absorbing potentials.

Comparison with a finite-basis approximation demonstrates that both left and right eigenvectors of the linear ($g = 0$) system must be taken into account to obtain correct values for the decay coefficients with a small number (e.g. two) of basis functions.

A time propagation of the eigenstates reveals that the states with linear counterpart (autochtonous states AuT and

Au+) evolve according to an adiabatic approximation based on the quasistationary resonance states for different values of the effective interaction $g \int_0^a |\psi(x)|^2 dx$. The time evolution of the allochtonous self-trapping state (AIT) can also be described by the adiabatic approximation until the bifurcation point is reached and the wavefunction starts to oscillate between the wells. For the allochtonous almost antisymmetric state (Al−) the wavefunction starts to oscillate immediately so that this state never evolves adiabatically. These results indicate that the self-trapping is not immediately destroyed by decay but is preserved on a time-scale determined by the decay coefficients of the respective self-trapping states. Furthermore, it was shown that these adiabatic stability properties can also be deduced from a linear stability analysis based on the Bogoliubov–de Gennes equations.

Acknowledgments

We would like to thank James R Anglin for valuable discussions. Financial support via the DFG Graduiertenkolleg 792 'Nichtlineare Optik und Ultrakurzzeitphysik' is gratefully acknowledged.

Appendix A. Resonance solutions of the linear Schrödinger equation with an open double-well potential

The Galerkin-type approach in section 3.3 requires the computation of the resonance eigenfunctions $u(x)$ and the corresponding eigenvalues $\mu - i\Gamma/2$ of the Hamiltonian H_0 given in equation (29) with the potential $V(x)$ given in equation (14), which are obtained by solving the stationary Schrödinger equation

$$\left(-\frac{\hbar^2}{2m}\partial_x^2 + V(x)\right)u(x) = (\mu - i\Gamma/2)u(x) \quad (\text{A.1})$$

with Siegert boundary conditions. The ansatz

$$u(x) = \begin{cases} \sin(kx) & 0 \leq x \leq b \\ (\sin(kb)/\sin(kb + \vartheta)) \sin(kx + \vartheta) & b < x \leq a \\ (\sin(kb)/\sin(kb + \vartheta)) \sin(ka + \vartheta) e^{ik(x-a)} & x > a \end{cases} \quad (\text{A.2})$$

with $k = \sqrt{2m(\mu - i\Gamma/2)}/\hbar$ already makes the wavefunction continuous at $x = a, b$ and satisfies the Siegert boundary condition $\lim_{x \rightarrow \infty} u'(x) = iku(x)$ as well as the boundary condition $u(0) = 0$. The matching conditions for the derivatives at $x = a, b$ read

$$k \cos(ka + \vartheta) = (ik - 2\lambda_a) \sin(ka + \vartheta) \quad (\text{A.3})$$

and

$$k \cos(kb) = k \frac{\sin(kb)}{\sin(kb + \vartheta)} \cos(kb + \vartheta) - 2\lambda_b \sin(kb), \quad (\text{A.4})$$

respectively. The complex quantities k and ϑ are obtained by solving these equations numerically. The wavefunction $u(x)$ diverges for $x \rightarrow \infty$ since $\text{Im}(k) < 0$. Therefore we use exterior complex scaling (see, e.g., [1, 47]) to make the wavefunction square integrable. The x coordinate is rotated by

an angle θ_c from the point where the potential $V(x)$ becomes zero. In our case this reads

$$x \rightarrow \begin{cases} x & x \leq a \\ a + (x - a) \exp(i\theta_c) & x > a. \end{cases} \quad (\text{A.5})$$

In the scaled region the Schrödinger equation becomes $\exp(2i\theta_c)u''(x) + k^2u(x) = 0$. Equations (A.3) and (A.4) remain unaltered. For a sufficiently large rotation angle θ_c the wavefunction $u(x)$ becomes square integrable in $0 \leq x < \infty$.

Because of $H_0 = H_0^T$, the complex conjugation of equation (32) shows that the corresponding left eigenfunctions $v(x)$ are given by $v(x) = (u(x))^*$. We normalize the eigenstates such that $\int_0^\infty dx v^*(x)u(x) = 1$.

References

- [1] Moiseyev N 1998 *Phys. Rep.* **302** 211
- [2] Glück M, Kolovsky A R and Korsch H J 2002 *Phys. Rep.* **366** 103
- [3] Syassen N, Bauer D M, Lettner M, Volz T, Dietze D, García-Ripoll J J, Cirac J I, Rempe G and Dürr S 2008 *Science* **320** 1329
- [4] Trompeter H, Pertsch T, Lederer F, Michaelis D, Streppel U, Brauer A and Peschel U 2006 *Phys. Rev. Lett.* **96** 023901
- [5] Trompeter H, Krolkowski W, Neshev D N, Desyatnikov A S, Sukhorukov A A, Kivshar Y S, Pertsch T, Peschel U and Lederer F 2006 *Phys. Rev. Lett.* **96** 053903
- [6] Musslimani Z H, Makris K G, El-Ganainy R and Christodoulides D N 2008 *Phys. Rev. Lett.* **100** 030402
- [7] Moiseyev N, Carr L D, Malomed B A and Band Y B 2004 *J. Phys. B: At. Mol. Opt. Phys.* **37** L193
- [8] Moiseyev N and Cederbaum L S 2005 *Phys. Rev. A* **72** 033605
- [9] Schlagheck P and Paul T 2006 *Phys. Rev. A* **73** 023619
- [10] Witthaut D, Mossmann S and Korsch H J 2005 *J. Phys. A: Math. Gen.* **38** 1777
- [11] Paul T, Richter K and Schlagheck P 2005 *Phys. Rev. Lett.* **94** 020404
- [12] Rapedius K, Witthaut D and Korsch H J 2006 *Phys. Rev. A* **73** 033608
- [13] Paul T, Hartung M, Richter K and Schlagheck P 2007 *Phys. Rev. A* **76** 063605
- [14] Rapedius K and Korsch H J 2008 *Phys. Rev. A* **77** 063610
- [15] Wimberger S, Schlagheck P and Mannella R 2006 *J. Phys. B: At. Mol. Opt. Phys.* **39** 729
- [16] Witthaut D, Graefe E M, Wimberger S and Korsch H J 2007 *Phys. Rev. A* **75** 013617
- [17] Graefe E M, Günther U, Korsch H J and Niederle A E 2008 *J. Phys. A: Math. Theor.* **41** 255206
- [18] Graefe E M, Korsch H J and Niederle A E 2008 *Phys. Rev. Lett.* **101** 150408
- [19] Anglin J 1997 *Phys. Rev. Lett.* **79** 6
- [20] Anglin J R and Vardi A 2001 *Phys. Rev. A* **64** 013605
- [21] Trimborn F, Witthaut D and Wimberger S 2008 *J. Phys. B: At. Mol. Opt. Phys.* **41** 171001
- [22] Morrison S and Parkins A S 2008 *Phys. Rev. A* **77** 043810
- [23] Morrison S and Parkins A S 2008 *J. Phys. B: At. Mol. Opt. Phys.* **41** 195502
- [24] Morrison S 2008 *Thesis* University of Innsbruck
- [25] Graefe E M and Korsch H J 2006 *Czech. J. Phys.* **56** 1007
- [26] Albiez M, Gati R, Fölling J, Hunsmann S, Cristiani M and Oberthaler M K 2005 *Phys. Rev. Lett.* **95** 010402
- [27] Schumm T, Hofferberth S, Andersson L M, Wildermuth S, Groth S, Bar-Joseph I, Schmiedmayer J and Krüger P 2005 *Nature Phys.* **1** 57
- [28] Gati R, Hemmerling B, Fölling J, Albiez M and Oberthaler M K 2006 *Phys. Rev. Lett.* **96** 130404
- [29] Gati R, Esteve J, Hemmerling B, Ottenstein T B, Appmeier J, Weller A and Oberthaler M K 2006 *New J. Phys.* **8** 189
- [30] Fölling S, Trotzky S, Cheinet P, Feld M, Saers R, Widera A, Müller T and Bloch I 2007 *Nature* **448** 1029
- [31] Theocharis G, Kevrekidis P G, Frantzeskakis D J and Schmelcher P 2006 *Phys. Rev. E* **74** 056608
- [32] Gottfried K 1966 *Quantum Mechanics* (New York: Benjamin)
- [33] Domcke W 1982 *J. Phys. B: At. Mol. Phys.* **15** 2675
- [34] Kok L P, de Maag J W and Brouwer H H 1982 *Phys. Rev. C* **26** 2381
- [35] Korsch H J, Möhlenkamp R and Meyer H D 1984 *J. Phys. B: At. Mol. Phys.* **17** 2955
- [36] Schlagheck P and Wimberger S 2006 *Appl. Phys. B* **86** 385–90
- [37] Siegert A J F 1939 *Phys. Rev.* **56** 750
- [38] Rapedius K, Elsen C B, Witthaut D and Korsch H J 2008 (in preparation)
- [39] Khomeriki R, Leon J, Ruffo S and Wimberger S 2007 *Theor. Math. Phys.* **152** 1122
- [40] Infeld E, Zin P, Gocalek J and Trippenbach M 2006 *Phys. Rev. E* **74** 026610
- [41] Li W D 2006 *Phys. Rev. A* **74** 063612
- [42] Korsch H J and Mossmann S 2003 *J. Phys. A: Math. Gen.* **36** 2139
- [43] Cartarius H, Main J and Wunner G 2008 *Phys. Rev. A* **77** 013618
- [44] Shibata T 1991 *Phys. Rev. B* **43** 6760
- [45] Morse P M and Feshbach H 1953 *Methods of Theoretical Physics* (New York: McGraw-Hill)
- [46] Castin Y and Dum R 1998 *Phys. Rev. A* **57** 3008
- [47] Zavin R and Moiseyev N 2004 *J. Phys. A: Math. Gen.* **37** 4619